The final publication is available at link.springer.com.
A. Abate and S. Boldo (Eds.): NSV 2017, LNCS 10381, pp. 90–97, 2017.
DOI: 10.1007/978-3-319-63501-9_7

Rigorous Reachability Analysis and Domain Decomposition of Taylor Models

Martin Berz and Kyoko Makino

Michigan State University, East Lansing MI 48824, USA
berz@msu.edu, makino@msu.edu,
WWW home page: http://bt.pa.msu.edu

Abstract. We present mathematically rigorous computational methods for the transport of large domains through ODEs with the goal of making rigorous statements about their long term evolution. Of particular interest are determination of locations of attractors, reachability of certain sets, and proof of non-reachability of others. The methods are based on Taylor model verified integrators for the propagation of large domains, and heavily rely on automatic domain decomposition for accuracy. We illustrate the behavior and performance of these methods using several commonly studied dynamical systems.

Keywords: Taylor model, verified ODE integration, domain decomposition, reachability analysis, incidence matrix

1 Introduction

Taylor model methods are rigorous computational tools that allow for the representation of functional dependencies via a floating point Taylor polynomial as well as rigorous bound of the accuracy of this representation over a given domain – see [1, 2] and references therein. Through the use of a naturally available antiderivation ∂_i^{-1} discussed in [2], it is possible to generate verified integrators for ODEs. In the single step, it can make use of a remarkably simple approach of rigorous enclosure of solutions of flows of ODEs, i.e. their dependence on initial condition and time, by porting the common Picard iteration scheme to the space of Taylor models [3]. Using several possible schemes for multi-steps, it is possible to achieve a far-reaching suppression of the wrapping effect (see for example [4–8] and many references therein) even in its manifestation in the remainder bound [9], which in itself is many orders of magnitude smaller than the main region covered by the flow.

Taylor model methods naturally allow for a domain decomposition approach in integration in a very similar way as it is used in many interval tools for global optimization (for a limited cross section of the many relevant books and papers, see [10–24] and references therein). In the case of optimization, the decision on whether or not to subdivide the region currently being studied, often referred to as the box, is made based on whether the box can be excluded because its known lower bound exceeds an already known upper bound for the minimizer. If

such an exclusion is not possible, the box is subdivided and each part is studied further.

On the other hand, in the case of verified integration, an excellent measure of whether a box is to be rejected is whether the remainder bound of the end result is unacceptably large, or whether the verified integrator tripped its internal failure tests for self inclusion in the integration process [3].

In the following, we will use this approach to determine the so-called incidence matrix, or alternatively a computational graph, for the flow of an ODE over a sufficiently large time domain, which can then be used for the analysis of asymptotic behavior of the solution.

2 Incidence Matrices, Graphs, and Reachability

We begin by splitting the domain of interest into n subsets covering the space, and numbering them as D_i. In practice they may consist of a collection of adjacent equally spaced boxes. We then define the so-called incidence matrix M associated with the splitting via

$$M_{i,j} = \begin{cases} 0 \text{ if it can be shown that } F(D_i) \cap D_j = \emptyset \\ 1 \text{ else} \end{cases} \tag{1}$$

where F is the flow of the ODE for the time step of interest.

So a value of 0 means that it is possible to show rigorously that an intersection does not exist. But note that in computational settings, the value 1 does not necessarily mean that there truly is an intersection, but rather it means that an intersection cannot be ruled out. The matrix can visually also be represented as a graph, where nodes denote the D_i, and vertices represent a value of 1 in the incidence matrix.

In practice it is very important that the matrix is usually rather sparse, and as the number of regions D_i is increased and the size of the D_i becomes smaller, the number of nonzero entries per D_i does usually not grow very much. This allows setting up rather large numbers of regions in the many millions, while the number of nonzero entries are only a moderate multiple of the number of entries. There is a significant body of literature related to the study of such graphs and the recovery of dynamics from it, for example [25–27] and references therein.

In the following we generate a simplified, domain decomposition based method for the determination of such a graph. For efficiency it is very important to not attempt to perform a verified integration for each of the D_i. Rather, we utilize a domain decomposing verified Taylor model integrator to first treat the entire region of interest covering all D_i, which results in a cover of the original domain space with a number of boxes that is much more manageable than the number of boxes D_i. In the next step, we identify all domain decomposed boxes in the initial domain that overlap with D_i. Then we compute a sharp enclosure for the true range of $f(D_i)$ by merely using a Horner scheme evaluation of the Taylor model for the small domain of D_i that is actually in the range of domain of the region of interest.

In the following we will provide various examples which clarify and illustrate the practical behavior of the method.

3 The Duffing Equation

As a first example, we consider the commonly studied Duffing equation

$$\ddot{x} + \delta\dot{x} + \alpha x + \beta x^3 = \gamma \cdot \cos(\omega t), \tag{2}$$

which models a damped and driven oscillator. The goal is the integration of large initial condition set for the Duffing equation of the form

$$\frac{dx}{dt} = y, \quad \frac{dy}{dt} = x - \delta \cdot y - x^3 + \gamma \cdot \cos t, \tag{3}$$

i.e. with the parameters

$$\delta = 0.25 \quad \text{and} \quad \gamma = 0.3. \tag{4}$$

The original domain box is

$$(x_i, y_i) \in ([-2, 2], [-2, 2]). \tag{5}$$

We show the case of integrating the Duffing equation from time $t = 0$ to $t = \pi$. The given initial condition set was initially equally divided into 12×12 pieces for purpose of better visibility of the action of the flow. Many initial condition subsets completed the entire time integration without any decomposition, and only those initial condition subsets located at the place where the strong nonlinearity exists during the requested integration exhibit decomposition. Since the Duffing equation is known to exhibit chaotic motion, very rich local dynamics results, as can be seen in Fig. 1, which shows the images of the resulting Taylor model solutions with decomposed Taylor model objects at $t = \pi$ (left), and the corresponding splits in the initial condition set (right). At the final time $t = \pi$, we count altogether 343 Taylor model objects. The increase of the number of Taylor model objects is graphed in Fig. 3, starting from $12 \times 12 = 144$ initially prepared objects.

We note that the Taylor models being used are of order 33 in time as well as in initial conditions. The CPU time on a midsize notebook computer is about 21 min, and 199 domain splits happened, resulting in a final number of 343 boxes. The smallest dimension of any of the resulting initial condition boxes has an edge length of $1/(3 \times 16)$.

For better illustration, a portion of the initial condition range consisting of $3 \times 3 = 9$ divided boxes and covering the region of $[-1, 0] \times [-1, 0]$, i.e. a piece located towards the lower left from the center $(0, 0)$, is shown in Fig. 2. For this portion of initial condition range, 24 splits happened, resulting in $9 + 24 = 33$ objects. The smallest division of the initial condition range size of $1/(3 \times 16)$ is easily observable in the x direction near the origin $(0, 0)$.

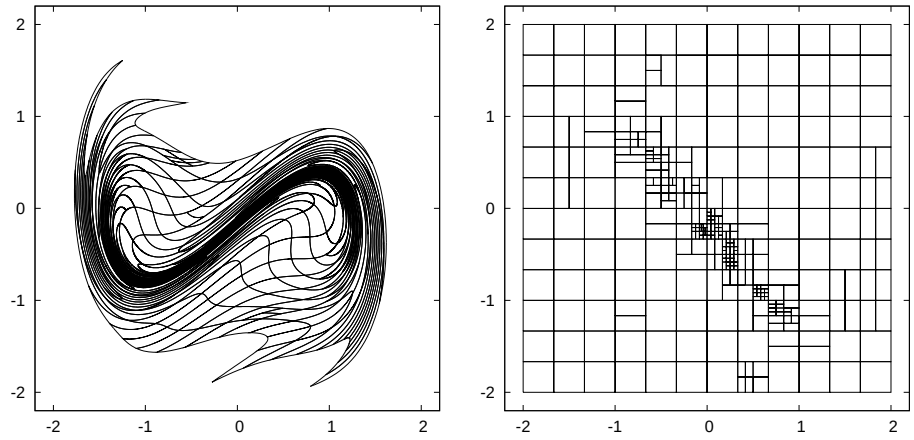

Fig. 1. Flow integration of the Duffing equation for the parameters show in the text. The right shows the original domain of interest, and the resulting subdivision of the domain in boxes that can successfully be transported. The left shows the images of the boxes under the flow. Note that the remainder error of the integration is below printer resolution and not visible in the examples.

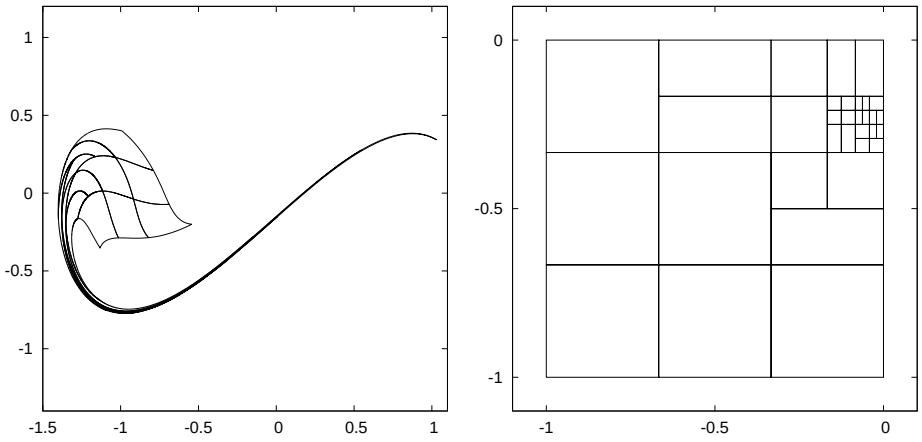

Fig. 2. A subset of the mapping of the original domain in a complicated region with much fine structure, showing that the automatic domain decomposition follows the computational local complexity of the flow.

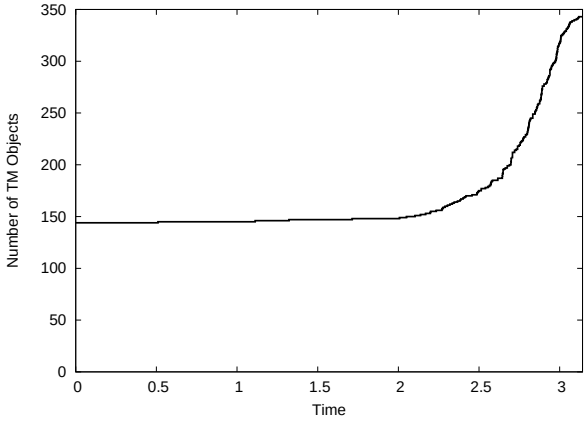

Fig. 3. Growth of the number of domain boxes as a function of integration time.

4 The Lorenz Equations

The next example discusses the Lorenz equations, which describe a simplified model of unpredictable turbulent flows in fluid dynamics. It is another frequently used example exhibiting sensitive dependence on initial conditions and chaoticity and has the form

$$\frac{dx}{dt} = \sigma(y - x), \quad \frac{dy}{dt} = x(\rho - z) - y, \quad \frac{dz}{dt} = xy - \beta z. \tag{6}$$

The standard parameter values are

$$\sigma = 10, \quad \beta = \frac{8}{3}, \quad \rho = 28, \tag{7}$$

and ρ is often varied. The fixed points are

$$(0, 0, 0), \quad (\pm\sqrt{\beta(\rho - 1)}, \pm\sqrt{\beta(\rho - 1)}, \rho - 1). \tag{8}$$

Rigorous flow integrations of large ranges of initial conditions have been computed using a Taylor model based ODE integrator.

In our example, we attempt a flow integration of the standard Lorenz equations for an area of initial condition

$$(x_i, y_i, z_i) \in ([-40, 40], [-50, 50], [-25, 75]), \tag{9}$$

which covers the entire region of interest for dynamics. In practice, this box of initial conditions is determined by heuristics so that an attractor is safely included inside.

The initial condition range box is pre-divided to $4 \times 5 \times 5 = 100$ smaller boxes to preserve a certain grid structure to guide the eye; so each of the original

domain boxes have the size $20 \times 20 \times 20$. The integration is conducted using the Taylor model computation order 21 in both time and initial conditions until $t = 0.1$. In the process, domain splitting happened 168 times, resulting in 268 objects. The minimum size experienced in the process is an initial condition box with edge width 5, 10, 10, respectively. The computation took 27 min including miscellaneous output for purposes of monitoring, the result, and files for plotting. Figure 4 shows a grid view of the result. The z axis is shown vertically upward, and at the bottom edges, the x axis is towards the right, and the y axis is towards the left.

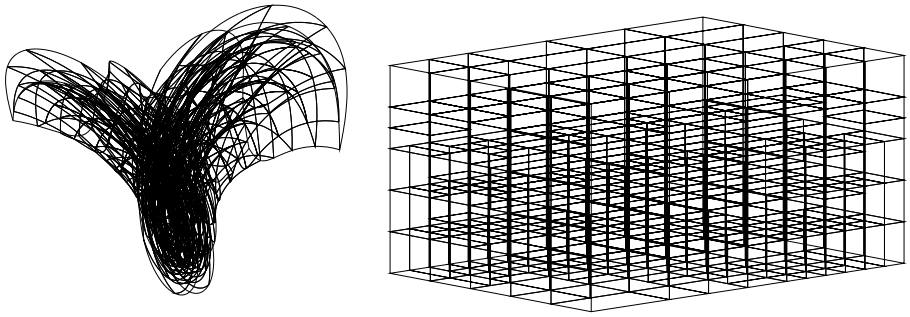

Fig. 4. Integration of the region of interest for the Lorenz system. Shown are the original domain of interest and the resulting subdivision of the domain in boxes that can successfully be transported at right, and the images of the boxes under the flow at left. Note that the remainder error of the integration is below printer resolution and not visible in the examples.

5 Conclusion

We have shown how it is possible to use Taylor model based self-verified integrators, when combined with automatic domain decomposition techniques usually used in global optimization, to obtain rigorous enclosures for flows of differential equations in an efficient manner. The resulting flow enclosures can be used to form incidence matrices of high fineness limited only by the size of the remainder bound of the Taylor models. Examples illustrating aspects of the method are given for two commonly used dynamical systems.

References

1. K. Makino. *Rigorous Analysis of Nonlinear Motion in Particle Accelerators.* PhD thesis, Michigan State University, East Lansing, Michigan, USA, 1998. Also MSUCL-1093.

2. K. Makino and M. Berz. Verified computations using Taylor models and their applications. In *NSV 2017*, Heidelberg, A. Abate, S. Boldo (eds.), *LNCS*, 10381:3-13, Springer, 2017.
3. K. Makino and M. Berz. Suppression of the wrapping effect by Taylor model-based verified integrators: The single step. *International Journal of Pure and Applied Mathematics*, 36,2:175–197, 2006.
4. R. J. Lohner. *On the Ubiquity of the Wrapping Effect in the Computation of Error Bounds*, pages 201–217. Springer, Berlin, 2001.
5. N. F. Stewart. A heuristic to reduce the wrapping effect in the numerical solution of ODEs. *BIT*, 11:328–337, 1971.
6. C. Barbarosie. Reducing the wrapping effect. *Computing*, 54:347–357, 1995.
7. W. Kühn. Rigorously computed orbits of dynamical systems without the wrapping effect. *Computing*, 61:47–67, 1998.
8. N. S. Nedialkov and K. R. Jackson. A new perspective on the wrapping effect in interval methods for IVPs for ODEs. *Proc. SCAN2000, Kluwer*, 2001.
9. K. Makino and M. Berz. Suppression of the wrapping effect by Taylor model-based verified integrators: Long-term stabilization by preconditioning. *International Journal of Differential Equations and Applications*, 10,4:353–384, 2005.
10. E. R. Hansen. Global optimization using interval analysis – the multidimensional case. *Numerische Mathematik*, 34:247–270, 1980.
11. J. Rokne H. Ratschek. *New Computer Methods for Global Optimization.* Ellis Horwood Limited, Chichester, England, 1988.
12. C. Jansson. A global optimization method using interval arithmetic. *IMACS Annals of Computing and Applied Mathematics*, 1992.
13. C. Jansson. A global optimization method using interval arithmetic. In *Computer Arithmetic and Scientific Computation, Proceedings of the SCAN 91*, Amsterdam, 1992. North–Holland, Elsevier.
14. H. Ratschek and J. Rokne. Interval tools for global optimization. *Computers Math. Applic.*, 21(6/7):41–50, 1991.
15. E. Hansen. *Global Optimization using Interval Analysis.* Marcel Dekker, 1992.
16. R. B. Kearfott. An interval branch and bound algorithm for bound constrained optimization. *J. Global Optim.*, 2:259–280, 1992.
17. R. Moore, E. Hansen, and A. Leclerc. Rigorous methods for global optimization. In *Recent Advances in Global Optimization (Princeton, NJ, 1991)*, Princeton Ser. Comput. Sci., pages 321–342. Princeton Univ. Press, Princeton, NJ, 1992.
18. M. A. Wolfe. On global optimization in R using interval arithmetic. *Optimization Methods and Software*, 3:61–76, 1994.
19. M. A. Wolfe. An interval algorithm for bound constrained global optimization. *Optimization Methods and Software*, 6:145–159, 1995.
20. E. Hansen and G. W. Walster. *Global Optimization using Interval Analysis.* Marcel Dekker, 2003.
21. K. Makino and M. Berz. Verified global optimization with Taylor model methods. *International Journal of Computer Research*, 12,2:245–252, 2003.
22. K. Makino and M. Berz. Range bounding for global optimization with Taylor models. *Transactions on Computers*, 4,11:1611–1618, 2005.
23. M. Berz, K. Makino, and Y.-K. Kim. Long-term stability of the Tevatron by validated global optimization. *Nuclear Instruments and Methods*, 558:1–10, 2006.
24. R. Armellin, P. Di Lizia, K. Makino, and M. Berz. Rigorous global optimization of impulsive planet-to-planet transfers in the patched-conics approximation. *Engineering Optimization*, 44:133–155, 2012.

25. C. Conley. *Isolated Invariant Sets and the Morse Index*. American Mathematical Society, Providence, Rhode Island, 1978.
26. J. Bush, M. Gameiro, S. Harker, H. Kokubu, and K. Mischaikow. Combinatorial-topological framework for the analysis of global dynamics. *Chaos*, 22:047508, 2012.
27. Z. Arai, W. Kalies, H. Kokubu, K. Mischaikow, H. Oka, and P. Pilarczyk. A database schema for the analysis of global dynamics of multiparameter systems. *Journal on Applied Dynamical Systems*, 8(3):757–789, 2009.